HHS Public Access

Author manuscript

Cell Rep. Author manuscript; available in PMC 2018 March 01.

Published in final edited form as:

Cell Rep. 2018 February 06; 22(6): 1531–1544. doi:10.1016/j.celrep.2018.01.041.

β-aminoisobutyric Acid, L-BAIBA, Is a Muscle-Derived Osteocyte Survival Factor

Yukiko Kitase[1,*], **Julian A. Vallejo**[2,3], **William Gutheil**[4], **Harika Vemula**[4], **Katharina Jähn**[5], **Jianxun Yi**[6], **Jingsong Zhou**[6], **Marco Brotto**[7], and **Lynda F. Bonewald**[1,8,9,*]

[1]Department of Anatomy and Cell Biology, School of Medicine, Indiana University, Indianapolis, IN 46202, USA

[2]Department of Biomedical Sciences, School of Medicine, University of Missouri-Kansas City, Kansas City, MO 64108, USA

[3]Department of Oral & Craniofacial Sciences, School of Dentistry, University of Missouri-Kansas City, Kansas City, MO 64108, USA

[4]Division of Pharmaceutical Sciences, School of Pharmacy, University of Missouri-Kansas City, Kansas City, MO 64108, USA

[5]Department of Osteology and Biomechanics, University of Medical Center Hamburg-Eppendorf, Hamburg, Germany

[6]Kansas City University of Medicine and Bioscience, Kansas City, MO 64106, USA

[7]Bone-Muscle Collaborative Science, College of Nursing & Health Innovation, University of Texas-Arlington, Arlington, TX 76019, USA

[8]Department of Orthopaedic Surgery, School of Medicine, Indiana University, Indianapolis, IN 46202, USA

SUMMARY

Exercise has beneficial effects on metabolism and on tissues. The exercise-induced muscle factor β-aminoisobutyric acid (BAIBA) plays a critical role in the browning of white fat and in insulin resistance. Here we show another function for BAIBA, that of a bone-protective factor that prevents osteocyte cell death induced by reactive oxygen species (ROS). L-BAIBA was as or more protective than estrogen or N-acetyl cysteine, signaling through the Mas-Related G Protein-Coupled Receptor Type D (MRGPRD) to prevent the breakdown of mitochondria due to ROS.

[*]Correspondence: kitasey@iu.edu (Y.K.), lbonewal@iu.edu (L.F.B.).
[9]Lead Contact

SUPPLEMENTAL INFORMATION

Supplemental Information includes Supplemental Experimental Procedures, five figures, and three movies and can be found with this article online at https://doi.org/10.1016/j.celrep.2018.01.041.

AUTHOR CONTRIBUTIONS

Conceptualization, Y.K. and L.F.B.; Methodology, Y.K., W.G., J.Z., M.B., and L.F.B.; Investigation, Y.K., J.A.V., J.Y., H.V., and K.J.; Writing, Y.K. and L.F.B.; Funding Acquisition, L.F.B. and J.Z.; Resources, W.G., J.Z., and L.F.B.; Supervision, W.G., Y.K., M.B., and L.F.B.

DECLARATION OF INTERESTS

The authors declare no competing interests.

BAIBA supplied in drinking water prevented bone loss and loss of muscle function in the murine hindlimb unloading model, a model of osteocyte apoptosis. The protective effect of BAIBA was lost with age, not due to loss of the muscle capacity to produce BAIBA but likely to reduced *Mrgprd* expression with aging. This has implications for understanding the attenuated effect of exercise on bone with aging.

Graphical abstract

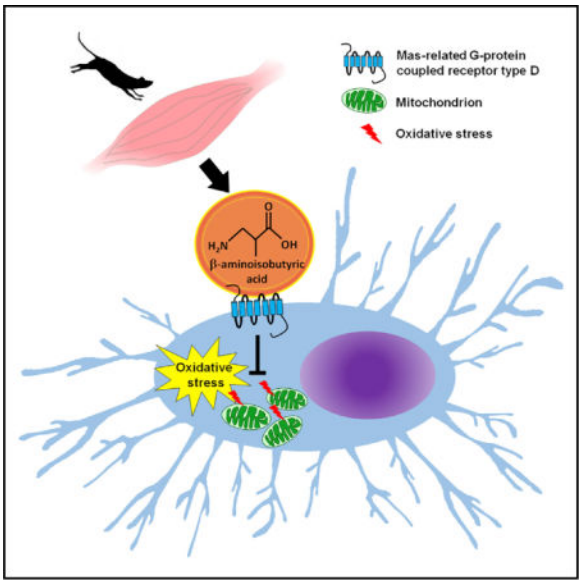

INTRODUCTION

Clearly, exercise has beneficial effects on many systems in the body, such as the neural, metabolic, and musculoskeletal systems (Blair et al., 1995, but it is not clear if these benefits delay the effects of aging or if aging blunts the effects of exercise. Sarcopenia and osteoporosis are major hallmarks of the aging musculoskeletal system, resulting in frailty, falls, fracture, and morbidity. It is predicted that 1 in 5 individuals will be over the age of 65 by 2020 (Benefield and Holtzclaw, 2014); therefore, it becomes imperative to understand these two co-morbidities in order to prevent both muscle and bone weakness.

Bone and muscle have an intimate relationship and show synchronization of tissue mass throughout life, from development to old age (Brotto and Bonewald, 2015). Exercise maintains or increases both bone and muscle mass, whereas disuse results in a reduction in mass/function of both tissues. Exercise has less of an anabolic effect on the bone with aging. Muscle and bone clearly have a mechanical interaction, with muscle loading the bone for locomotion, but recently it has been shown these tissues communicate through secreted factors. Factors have been identified as secreted by bone cells, such as osteocalcin (Karsenty and Olson, 2016), and secreted by osteocytes, such as prostaglandins (Mo et al., 2012) and WNTs (Huang et al., 2017), which have effects on muscle. Contracted muscle-derived factors, such as insulin growth factor-1 (IGF-1), fibroblast growth factor-2 (FGF-2) (Hamrick et al., 2010), interleukin-15 (IL-15) (Nielsen et al., 2007), and irisin (Colaianni et

al., 2015), have osteogenic effects. In contrast, disuse-induced muscle atrophy produces myostatin that has anti-osteogenic effects by decreasing osteoblastogenesis (Qin et al., 2017) and increasing osteoclastogenesis (Dankbar et al., 2015). These findings support the concept of muscle/bone communication.

Our group has focused on the bone cell embedded in the bone matrix, the osteocyte. Osteocytes derive from a subpopulation of osteoblasts by the embedding into the newly formed bone and the formation of a global mechanosensory cellular network inside the bone matrix. This cell has come from obscurity a decade ago to being recognized as a multifunctional cell (Bonewald, 2011) that can regulate osteoclasts, the bone-resorbing cells, through RANKL expression (Nakashima et al., 2011; Xiong et al., 2015), and osteoblasts, the bone-forming cells, through sclerostin production (van Bezooijen et al., 2004) and WNT1 (Joeng et al., 2017). Osteocytes as endocrine cells have been shown to target the kidney through fibroblast growth factor-23 (Feng et al., 2003) by binding the FGF receptor/Klotho complex (Urakawa et al., 2006) to regulate phosphate excretion by the kidney. Unlike osteoblasts and osteoclasts, which are viable from days to a few weeks, osteocytes are viable for decades in the bone matrix. Osteocyte death can signal resorption and remodeling of bone; therefore, maintenance of osteocyte viability requires tight control. A number of factors have been shown to cause osteocyte cell death, such as IL-1, tumor necrosis factor alpha (TNF-α), glucocorticoids, reactive oxygen species (ROS), and others, and to prevent the effects of these factors, a number of protective factors have been shown to prevent osteocyte cell death, such as estrogen, parathyroid hormone, N-acetyl cysteine (NAC), and others (Jilka et al., 2013). However, these protective factors are not regulated by exercise, so we postulated that muscle secretes osteocyte-protective factors in response to contraction. We had previously shown that muscle is a source of osteocyte-protective factors, and we showed that contracted muscle secretes factors that protect osteocytes against glucocorticoid-induced cell death (Jähn et al., 2012). Here we identify β-aminoisobutyric acid (BAIBA) as a major osteocyte-protective factor.

In 2014, BAIBA was described as a small (103.6-Da) molecule produced by skeletal muscle during exercise (Roberts et al., 2014), and it was shown to signal the beneficial effect of exercise from skeletal muscle to other tissues and organs in an endocrine manner. BAIBA increases energy expenditure by activating the β-oxidation pathway of hepatic fatty acid, triggers the browning of white adipose tissue, is inversely correlated with cardiometabolic risks factors (Roberts et al., 2014), and improves insulin resistance and inflammation in skeletal muscle in an autocrine/paracrine manner (Jung et al., 2015). More recently, the molecule has been shown to reduce hepatic endoplasmic reticulum (ER) stress and glucose/lipid metabolic disturbance in type 2 diabetes (Shi et al., 2016) and to ameliorate renal fibrosis, in a mouse model of obstructed kidney, via the inhibition of renal fibroblast activation and fibrosis (Wang et al., 2017).

Here we describe another function for BAIBA as a muscle-secreted factor that protects osteocytes against ROS and can prevent both bone and muscle loss *in vivo*. We identified and describe the mechanism used by this factor to protect osteocytes, via signaling through the Mas-related G protein-coupled receptor type D (MRGPRD), to prevent mitochondrial breakdown in osteocytes. We also describe how this function of BAIBA is lost with aging,

not through the muscle capacity to produce BAIBA with contraction but through the downregulation of this receptor in osteocytes. These findings have implications for correcting reduced skeletal response to exercise with aging and for muscle-bone interactions during aging.

RESULTS

Muscle Secretes Osteocyte-Protective Factors

Previously we hypothesized that muscle and bone communicate through soluble factors (Bonewald et al., 2013), and then we showed that osteocytes produce factors that support myogenesis and muscle function (Mo et al., 2012) and that muscle secretes osteocyte-protective factors (Jähn et al., 2012). As C2C12 myotube conditioned media (CM) mimicked the effects of extensor digitorum longus (EDL) and soleus (SOL) CM (Figure 6 of Jähn et al., 2012) with regard to osteocyte-protective capability, a series of fractionation experiments were performed. The bioactivity was less than 10 kDa (even less than 3 kDa), resistant to trypsin and boiling, and partially degraded by UV light over time (Figures S1A and S1B). As we have demonstrated previously that PGE_2 is a potent anti-apoptotic agent and is highly expressed by osteocytes in response to fluid flow shear stress (Kitase et al., 2010), we measured PGE_2 levels in muscle CM. CM from C2C12 myoblasts or myotubes and both EDL and soleus with and without contraction presented with low levels of PGE_2, insufficient to have an effect on osteocytes (MLO-Y4 cells subjected to 2 dynes/cm^3 fluid flow shear stress produced 18,353 ± 1,969, C2C12 myotube-CM 168 ± 10, and C2C12 myoblast-CM 63 ± 4 PGE_2 pg/10^6 cells; experiments were repeated 3 times with similar results).

As ROS are elevated with aging, we next determined if muscle-secreted factors could protect against ROS-induced osteocyte cell death. Both static and contracted EDL and soleus CM were protective (Figure S2). We screened a number of small molecular weight molecules secreted by muscle, including BAIBA, for their protective capacity using the osteocyte cell line MLO-Y4, and BAIBA was the most potent (Figure 1A). The L-isoform was shown to be the more active form compared to the D-isoform (Figure 1A), and L-BAIBA was as or more potent than the well-known anti-apoptotic factors β-estradiol and NAC (Figure 1B). ROS was shown to be reduced by both L-BAIBA and the positive control NAC (Figure 1C). Catalase and Gpx4, known to protect against ROS, were increased in response to L-BAIBA, similar to NAC (Figure 1D). We have also examined the protective effect of BAIBA on osteoblasts as precursors of osteocytes using an osteoblast cell model, MC3T3-E1, and we found that it also prevented them from cell death induced by hydrogen peroxide (Figure S3).

L-BAIBA Protects against Bone and Muscle Loss due to Disuse

To understand the *in vivo* relevance of the cellular effects determined *in vitro*, experiments were performed using the established murine hindlimb unloading model in which the detrimental effects of unloading on bone mass through apoptotic osteocytes is well described (Basso and Heersche, 2006). Blocking osteocyte apoptosis using an apoptosis inhibitor has been shown to prevent bone loss induced by hindlimb unloading (Cabahug-Zuckerman et al., 2016). As BAIBA production is increased with exercise (Roberts et al., 2014), the hindlimb unloading assay, a model for disuse or lack of exercise, was performed to determine if

BAIBA could prevent bone loss. Hindlimb unloading was performed for 2 weeks on paired 5-month-old males or 3-month-old females with or without 100 mg/kg/day L-BAIBA added to drinking water (3-month-old females were chosen because of almost complete loss of trabecular bone by 5 months of age).

At baseline, both groups showed no statistical differences in trabecular parameters in the tibial metaphysis. Also at baseline, both groups showed no statistical differences in Ellipsoid factor (EF) values categorized in each structure showing plate-type-dominated structures (control, 50.3% ± 6.8%; L-BAIBA, 45.1% ± 7.6% in male; control, 31.2% ± 11.4%; L-BAIBA, 38.912.42% in female) and intermediate structures (control, 49.5% ± 6.8%; L-BAIBA, 54.4% ± 7.8% in male; control, 64.0% ± 11.7%; L-BAIBA, 59.8% ± 15.4% in female). *In vivo* micro computed tomography (μCT) analysis at two time points showed that hindlimb-unloaded mice given L-BAIBA have significantly higher bone volume fraction (BV/TV), and higher thickness and connectivity of trabecular bones compared to control group that was gender-independent (Figures 2A–2E). *Ex vivo* μCT analysis confirmed the *in vivo* μCT data (Figures 2F–2J). EF analysis revealed more plate-type-dominated structures retained in males after 2-week hindlimb unloading, while bone in the control group shifted to more intermediate structures. No differences in EF analysis in female mice were observed (Figures 2K–2N). By histological analysis, bone parameters were generally consistent with μCT data as shown in Figure 2, and, while there was no effect on osteoclast parameters in both males and females, osteoblast number and surface were significantly higher in male L-BAIBA-treated animals (Figures 3A–3H). Similar to the *ex vivo* μCT data shown in Figure 2, there was a significant difference, higher BV/TV, trabecular number (Tb.N), and trabecular thickness (Tb.Th.) and lower trabecular separation (Tb.Sp.), in treated compared to control males. Unlike the μCT data in Figure 2, no significant differences were observed in bone parameters in females. Significantly greater apoptosis was observed in osteocytes in the untreated as compared to the L-BAIBA-treated animals (Figure 3I). Real-time PCR did not show a significant change in *Rankl*, *Opg*, and *Sost* mRNA obtained from femurs (Figure 3J).

To determine if the administration of L-BAIBA has an additional effect on muscle function in the disuse model, *ex vivo* contractility of the EDL (mainly consisting of glycolytic muscle fibers) and of the soleus (mainly consisting of oxidative muscle fibers) muscles was performed. EDL showed significantly greater muscle mass and maximal tetanic force in male mice receiving L-BAIBA over controls (Figures 4A and 4B). A significant difference in soleus half-maximal force and rate of force development was observed in L-BAIBA-treated males (Figures 4H and 4J). Additionally, the force-frequency relationship of soleus from male mice treated with L-BAIBA showed higher relative forces at stimulatory frequencies in the range of 40–80 Hz compared to non-treated controls (Figure 4L). Interestingly, EDL and soleus muscles from female mice were virtually unaffected by L-BAIBA treatment (Figures 4A–4L).

L-BAIBA Is Produced by Both Young and Old Contracted Muscle

To determine if BAIBA is produced by both young and aged muscle, CM were obtained from both EDL and soleus muscles dissected from male and female mice, 5 and 22 months

old, with and without contraction at 90 Hz. Muscle CM were freeze-dried, derivatized using Marfey's reagent, and then quantitated by liquid chromatography-mass spectrometry (LC-MS) as described previously (Vemula et al., 2017). Contraction stimulated L-BAIBA production in all muscle, EDL and soleus, male and female, but to a greater extent in aged muscle compared with young muscle (Figure 5A). There were no significant changes in 20 amino acids or in the BAIBA analogs, such as γ-aminobutyric acid (GABA) (Figures S4A and S4B).

L-BAIBA Protects Young, but Not Old, Osteocytes from ROS-Induced Cell Death

To begin to determine if BAIBA might function as an osteocyte-protective agent with aging, osteocytes from both 5- and 22-month-old male and female mice were tested. L/D-BAIBA and L-BAIBA blocked the negative effects of ROS on young, but not old, osteocytes (Figures 5B and 5C).

L-BAIBA Signals through the MRGPRD to Protect Osteocytes from Cell Death

As old muscle was just as capable as young muscle to secrete L-BAIBA in response to contraction, we asked if the receptor for BAIBA could be affected by aging. Mas-related G protein-coupled receptor type D (*Mrgprd*) and glycine receptors, both known BAIBA receptors, were examined in primary bone cells. The *Mrgprd* was highly expressed in primary osteocytes especially at 5 months of age (Figure 6A). Expression increased from 2.5 months to 5 months and highly decreased by 22 months of age. The expression level was higher in males compared to females. These receptors were more highly expressed in the primary osteocyte population compared to primary osteoblasts (Figure 6A). Glycine receptors (*Glra4* and *Glrb*) were expressed at lower levels than the *Mrgprd* (Figure 6B). Even though the *Glrb* was highly expressed in MLO-Y4 cells, there was a little expression of its potential subunit, *Glra4*, that was dimerized to form their functional receptor (Figure 6C). *Glra1–3* were not detectable. Other ligands for these receptors include β-alanine and GABA, so these were compared to L-BAIBA for osteocyte-protective capacity. L-BAIBA was approximately 100-fold more potent than β-alanine, GABA, or glycine (Figure 6D). To determine if MRGPRD is the functional receptor for BAIBA, inhibitory assays were performed. The receptor antagonist for MRGPRD, MU6840, significantly attenuated the activity of L-BAIBA (Figure 6E). Experiments were performed using small interfering RNA (siRNA) and CRISPR technology for knockdown studies. *Mrgprd*-targeted siRNA was shown to completely block the expression of mRNA (Figure 6F) and reverse the positive effects of L-BAIBA on H_2O_2-induced cell death (Figure 6G). Two different *Mrgprd* single guide RNAs (sgRNAs) were shown to significantly reduce protein expression of MRGPRD (Figure 6H) and to significantly block the positive effects of L-BAIBA on H_2O_2-induced cell death (Figure 6I). Therefore, based on inhibitor and knockdown studies, the MRGPRD appears to be the receptor mediating the protective effects of L-BAIBA on osteocytes.

Mitochondria Movement and Dynamics in Osteocytes

Next, we asked how L-BAIBA maintains osteocyte viability. Osteocytes have been imaged previously *in vivo* for active mitochondria using Tetramethylrhodamine, ethyl ester, *TMRE*, a cell-permeant, cationic, red-orange fluorescent dye that is readily sequestered by active mitochondria (Frikha-Benayed et al., 2016). These investigators suggested that osteocytes

with impaired mitochondrial function may be more susceptible to apoptosis. As mitochondria are known to produce ROS as a by-product along with the production of ATP, we decided to determine if mitochondria might be involved in the protective effects of BAIBA on H_2O_2-induced cell death. Using Mito Red, we found that mitochondria can be imaged over time in MLO-Y4 cells and mitochondria can be observed moving in the dendritic processes, similar to that observed with oligodendrocyte primary processes and neuronal dendrites (Rinholm et al., 2016) (Figure 7A; Movies S1 and S2). Primary osteocytes isolated from Dmp1-GFP mice showed similar properties with regard to mitochondrial movement (Figure 7A; Movie S3).

L-BAIBA Prevents Mitochondrial Breakdown due to ROS

To determine if L-BAIBA would prevent the negative effects of ROS on mitochondria, time-lapse imaging experiments were performed. When H_2O_2 (100 μM) was applied to MLO-Y4 osteocyte-like cells, unopposed fission occurred over 50 min along with reduced TMRE intensity (Figure 7B), but this effect was blocked by L-BAIBA (Figures 7C and 7D). To quantitate the mitochondrial functional status, cells were stained with TMRE, which is fluorescent only in functional mitochondria, and with mitoD, which stays fluorescent whether the mitochondria are functional or not. The ratio of TMRE/mitoD, which is related to mitochondrial membrane potential, is shown in Figures 7E–7G. This ratio was significantly reduced with H_2O_2, while L-BAIBA pretreatment maintained the same ratio in response to H_2O_2 as non-treated cells. Therefore, L-BAIBA appears to protect osteocytes through the maintenance of their mitochondria. Not only does L-BAIBA have short-term effects on mitochondria integrity but also it regulates mitochondrial gene expression (Figure S5).

DISCUSSION

The effects of muscle on bone were previously thought to be exclusively mediated through mechanical loading, however, here we show that, in addition, the muscle can have effects on bone through a secreted metabolite, BAIBA. Others have shown that muscle can secrete factors that have effects on other tissues. Originally these factors were termed myokines and shown to be secreted proteins (Pedersen, 2011). Exercise has been shown to stimulate skeletal muscle to secrete soluble factors that modulate bone metabolism, such as IGF-1 and FGF-2 (Hamrick et al., 2010) and irisin, which has been shown to increase bone mass (Colaianni et al., 2015). We proposed that muscle would secrete proteins that would protect osteocytes from cell death (Jähn et al., 2012), but we found a small molecular weight molecule, a metabolite, was responsible. Both the slow-twitch oxidative muscle, such as soleus, and fast-twitch glycolytic muscles, such as EDL, secrete BAIBA when contracted. BAIBA was found to be as or more potent than known protective factors β-estradiol and NAC.

BAIBA is a small molecule produced by skeletal muscle during exercise (Roberts et al., 2014). BAIBA consists of two enantiomers, L-BAIBA and D-BAIBA. This non-protein β-amino acid, L-BAIBA, is produced from the utilization of a branched amino acid L-valine as an energy source under the control of transcriptional co-activator PGC-1α. BAIBA was

shown to be a mediator of the beneficial effect of exercise from skeletal muscle to other tissue organs in an endocrine manner. It activates the β-oxidation pathway of hepatic fatty acid, and it triggers the browning of white adipose tissue (Roberts et al., 2014), improves insulin resistance and inflammation in skeletal muscle in an autocrine/paracrine manner (Jung et al., 2015), prevents diet-induced obesity (Begriche et al., 2008), and protects against metabolic disturbance in type 2 diabetes (Shi et al., 2016). We have now shown another function for this muscle metabolite, that of protecting osteocytes from cell death. *In vivo*, this metabolite retains bone and muscle with unloading apparently through this mechanism.

Every amino acid except glycine has two enantiomers. Usually naturally occurring amino acids in cells are the L-form, not the D-form. However, D-BAIBA is derived from thymine and excluded in the urine (Smith and Dymond, 1963). We determined the greater potency of the L-form compared to the D-form on osteocyte viability (Figure 1A). We have also shown that L-BAIBA, but not D-BAIBA, is produced by contracted muscle regardless of skeletal muscle type, gender, and age (Figure 5A). As far as we know, the different enantiomers have not been tested on the MRGPRD signaling, but, based on our results, it is assumed that the L-form is the biologically active form that binds to this receptor.

Osteocytes are one of the longest-lived cells in the body, remaining viable in the bone matrix for decades (Manolagas and Parfitt, 2013). Osteocyte viability is crucial for the normal functioning of the skeleton and potentially for the normal function of other organs, such as kidney and muscle. Osteocytes are multifunctional cells that regulate bone remodeling through osteoblasts and osteoclasts, act as endocrine cells targeting other tissues, regulate both calcium and phosphate homeostasis, and also act as mechanosensory cells that signal for bone removal with disuse and bone formation with anabolic loading (Bonewald, 2011; Dallas et al., 2013).

Programmed osteocyte cell death is necessary to repair damaged bone (Kennedy et al., 2012; Verborgt et al., 2000, 2002). This type of osteocyte cell death acts as a beacon to direct osteoclasts to the microdamaged bone for removal as the osteocytes sacrifice themselves in order to repair bone. This process is highly programmed to release factors, such as RANKL, to direct osteoclasts to damaged sites for repair. Therefore, it is important to maintain the health and function of the osteocyte to maintain bone homeostasis. However, as we age, these cells begin to die and their remains are removed and lost through the lacuno-canalicular system, leaving empty lacunae, or the dying cells can vesiculate and micropetrose, resulting in a mineralized filling in of their lacunae (for reviews on osteocytes, see Bonewald, 2011 and Dallas et al., 2013). This results in a compromised lacuno-canalicular system with impaired osteocyte signaling.

BAIBA was reported to bind to glycine receptors and to the MRGPRD, which is also known to be a receptor for β-alanine, and the neurotransmitter GABA (Uno et al., 2012). The *Mrgprd* is most highly expressed in nonpeptidergic dorsal root ganglia neurons (Zylka et al., 2005) and found to be the sensory receptor for irritation, such as noxious mechanical stimuli (Cavanaugh et al., 2009). Protein expression was only found in dorsal root ganglia (McNeil and Dong, 2014), but low mRNA levels were detected in bladder, uterus, testes, arteries, and femur (Shinohara et al., 2004). We found that an MRGPRD antagonist, MU6840 (Uno et al.,

2012), blocked the beneficial effect of L-BAIBA ROS-induced cell death, as did both siRNA and sgRNA to *Mrgprd*. Whereas muscle from both young, 5-month-old, and 22-month-old mice produce BAIBA in response to contraction, osteocytes from old mice are not protected by BAIBA to the same extent as young osteocytes. *Mrgprd* was highly expressed in young osteocytes but decreased in expression in old osteocytes. This suggests that osteocytes lose their response to BAIBA with aging. Aged contracted muscle can produce BAIBA in response to exercise, but the reduction in receptor expression may reduce the beneficial effects of exercise on osteocytes.

A number of factors have been shown to induce osteocyte cell death, including glucocorticoids and cytokines such as IL-1 and TNF-α. Conversely, a number of molecules have been shown to protect osteocytes from cell death, including estrogen and bisphosphonates (for review, see Bellido and Plotkin, 2011; Jilka et al., 2013; Jilka and O'Brien, 2016). We showed that secreted muscle factors could protect osteocytes from glucocorticoid-induced cell death and that this effect was mediated through the β-catenin-signaling pathway (Jähn et al., 2012). It has been suggested that oxidative stress caused by disuse, estrogen deficiency, excess corticosterone, and aging may be responsible for bone cell death and, therefore, bone fragility (Almeida and O'Brien, 2013). Here we performed studies examining the effects of ROS, known to be generated with aging, on osteocyte viability. Mitochondria play a crucial role in cell survival. Mitochondria require ROS for normal function (Holzerová and Prokisch, 2015), but with aging excess ROS leads to mitochondrial breakdown (Finkel, 2015; Valko et al., 2007). During apoptosis, alteration of mitochondrial structure and reduction of membrane potential are present. Mitochondria show massive fragmentation of their network associated with cytochrome *c* release, which induces the formation of the apoptosome leading to activation of caspase-3, responsible for apoptosis (Langlais et al., 2015). We were able to image mitochondria in both MLO-Y4 cells and primary osteocytes, showing trafficking similar to that observed in axonal neural cells (Rinholm et al., 2016). Here we show that BAIBA prevented or reduced this massive breakdown of mitochondria induced by H_2O_2 in MLO-Y4 osteocyte-like cells.

As BAIBA production is increased with exercise (Roberts et al., 2014) and with contraction of isolated EDL and soleus as shown in this study, the hindlimb unloading assay, a model of disuse or lack of exercise, was performed to determine the effects of L-BAIBA on both bone and muscle. The detrimental effects of unloading on bone mass through osteocytes are well described (Basso and Heersche, 2006), and it has previously been shown that blocking osteocyte apoptosis prevents bone loss due to hindlimb unloading (Cabahug-Zuckerman et al., 2016). We found that providing L-BAIBA in drinking water for 2 weeks of hindlimb unloading retained bone mass, more so in males than females, most likely due to the greater amount of trabecular bone in males compared to females even with using 3-month-old females as compared to 5-month-old males. By histomorphometric analysis, more bone was retained in males given L-BAIBA, but this was not observed in females, most likely due to the low amount of trabecular bone, which can be more easily quantitated using 3-dimensional μCT, but not 2-dimensional bone histomorphometry. Also, significantly greater apoptosis was observed in osteocytes in the untreated as compared to the L-BAIBA-treated animals, whereas no differences were observed in mRNA for the osteocyte factors, sclerostin, Rankl, or osteoprotegerin. These data suggest that L-BAIBA protects both

osteoblasts and osteocytes through maintenance of viability and not through regulation of osteoblasts via sclerostin and osteoclasts via Rankl/Opg. L-BAIBA could potentially be exerting a direct effect on osteoblasts, but, as osteocytes express much higher levels of *Mrgprd*, the effects on osteoblasts could be indirect through the maintenance of osteocyte viability.

Male mice treated with L-BAIBA during hindlimb unloading retained EDL muscle mass and maximal contractile force over controls, however, EDL maximal force normalized to muscle size was similar between groups, indicating that the higher EDL mass in the L-BAIBA-treated group accounted for the higher contractile force. Soleus muscles from L-BAIBA-treated mice displayed higher contractile force and rate of force development at stimulatory frequency, which produces approximately half of maximal contractile force output (40 Hz) as well as a leftward shift in the force-frequency curve at 40–80 Hz over controls. The force-frequency profile is indicative of muscle fiber myosin heavy chain (MHC) composition, with slow type 1 muscle fibers displaying higher Ca^{2+} sensitivity as well as the higher rates of calcium sarcoplasmic reticulum (SR) release at these lower frequencies of stimulation and, therefore, higher relative forces at suboptimal frequencies compared to fast type 2 MHC-enriched muscle fibers. Enhanced muscle contractility at these lower frequencies is very physiologically relevant, especially when considering that mammalian skeletal muscles normally function in this range (Edwards et al., 1977a, 1977b). These studies also demonstrate that muscle mass does not necessarily directly correlate with function, therefore, function can be preserved despite no gains in muscle mass. Interestingly, EDL and soleus muscles from female mice were virtually unaffected by L-BAIBA treatment. These differences in response to L-BAIBA could be due to the combined effects of higher estrogen expression levels and lower testosterone concentrations in combination with the higher docosahexaenoic acid (DHA) in the female's body, as observed in humans (Bakewell et al., 2006; Giltay et al., 2004).

Based on these observations, one might speculate that BAIBA may exert not only direct effects on bone cells but also indirect effects by preserving muscle that directly loads the tibia, especially in male mice. Retention or preservation of both mechanical stimuli and secreted myokines such as BAIBA may act together to preserve bone mass. In the EDL muscle composed of different muscle fiber types, L-BAIBA may be acting through preservation of muscle mass. Muscle disuse is known to lead to shifts in MHC expression from slow MHC type 1 to faster MHC type 2 isoforms in slow-twitch muscles like the soleus. BAIBA has been found to induce expression of peroxisome proliferator-activated receptor delta (PPARδ) in skeletal muscle (Jung et al., 2015), a known regulator of slow type 1 muscle fiber development/maintenance (Ehrenborg and Krook, 2009). This suggests that L-BAIBA may attenuate disuse-induced fiber type switching in soleus muscle via the induction of PPARδ expression. The autocrine effects of BAIBA on muscle will require additional investigation, especially in the context of bone and muscle crosstalk.

In summary, we have identified another function for the muscle-derived metabolite L-BAIBA on osteocyte viability. L-BAIBA protects osteocytes from ROS-induced apoptosis through the MRGPRD and through maintaining mitochondria integrity. This protective capacity appears lost with aging due to the downregulation of *Mrgprd* expression in

osteocytes. Therefore, targeting receptor expression in osteocytes with aging may return the bone anabolic response to exercise.

EXPERIMENTAL PROCEDURES

Please refer to the Supplemental Experimental Procedures for a detailed description of other experiments.

MLO-Y4 Cells

The osteocyte-like MLO-Y4 cell line, derived from murine long bone, was used as an *in vitro* osteocyte model (Kato et al., 1997). MLO-Y4 cells were maintained on collagen type I-coated plates in α-MEM supplemented with 2.5% fetal bovine serum (FBS), 2.5% calf serum (CS), and 100 U/mL penicillin/streptomycin (P/S) in a 5% CO_2 incubator at 37°C. For all assays, phenol red-free a-MEM was used.

Isolation of Primary Bone Cells from Mouse Long Bones

Primary bone cells were isolated as previously described with some modifications (Stern et al., 2012). Briefly, long bones were dissected from 5- or 22-month-old C57BL/6 male mice for cell death assay and from 3-month-old DMP1-GFP female mice for live imaging. After removal of soft tissue, epiphyses were cut off and bones were flushed with PBS using a 27G½ needle-syringe to remove bone marrow. Bones were then longitudinally cut and digested 3 times with 300 U/mL collagenase type IA (Sigma-Aldrich, C9891), one time with 5 mM EDTA (Sigma-Aldrich, E5134)/0.1% BSA (Sigma-Aldrich, A7030), and one more with the collagenase, each for 25 min at 37°C. The bones were minced into small pieces and cultured in 5% FBS/5% CS/α-MEM in a 6-well plate coated with 0.15 mg/mL rat tail collagen type I (Corning, 354236) until primary bone cells were obtained as an outgrowth from the bone chips.

Quantification of Cell Death

MLO-Y4 cells or primary bone cells obtained from long bones were plated at 1−1.25 × $10^4/cm^2$ on a collagen-coated 96-well plate with 6 wells for each experimental condition. Representative examples of two or four independent experiments are shown. Cells were pretreated with varying concentrations of L/D-BAIBA (Sigma-Aldrich, 217794), L-BAIBA (Sigma-Aldrich, 51511), D-BAIBA (Sigma-Aldrich, 68337), β-estradiol (Sigma-Aldrich, E8875), NAC (Sigma-Aldrich, A7250), β-alanine (Sigma-Aldrich, 146064), or GABA (Sigma-Aldrich, A2129) in 1% FBS/1% CS/α-MEM for 1 or 24 hr, followed by treatment with 0.3 mM hydrogen peroxide (EMD Millipore, HX0635-3) for 3–4 hr in 0.5% FBS/0.5% CS/α-MEM to induce 20%–40% cell death. The cells were pretreated with MU6840 (Key Organics, 5R-0328) for 30 min before adding L-BAIBA. Cells were stained with 2 μM ethidium homodimer 1 (EthD-1, Invitrogen, E1169) for 30 min and analyzed on a Nikon Eclipse TE300 inverted fluorescence microscope to detect dead cells. Images were acquired under 10× magnification using epifluorescence illumination with a Photometrics Coolsnap EZ cooled charge-coupled device (CCD) camera interfaced with ImageJ, and we quantified thresholded images using a function of particle analyzer in ImageJ (NIH). Percentage of cell death was calculated as EthD-1-positive cells divided by the total number of cells stained

with 5 μg/mL Hoechst 33342 (Invitrogen, H1399) as a nuclear counterstain. Data are presented as fold change over the level of cell death in the sample treated with hydrogen peroxide alone.

Mice

2.5-, 3-, 5-, and 22-month-old C57BL/6 female and male mice were obtained from Charles River or the National Institute of Aging animal colony. All animal experiments were performed according to an approved Institutional Animal Care and Use Committee protocol at the University of Missouri-Kansas City (UMKC), conforming to relevant federal guidelines. The UMKC animal facility is operated as a specific pathogen-free, AAALAC-approved facility. Animal care and husbandry meet the requirements in the Guide for the Care and Use of Laboratory Animals by the National Research Council. Animals were group housed and maintained on a 12-hr light/dark cycle with *ad libitum* food and water at a constant temperature of 23°C. Daily health check inspections were performed by qualified veterinary staff and/or animal care technicians.

Hindlimb Unloading with or without L-BAIBA

Paired 5-month-old male mice from the same litter (total 6 pairs from 3 litters) or paired 3-month-old female mice from the same litter (total 6 pairs from 4 litters) were assigned to either control or treated and housed in one large cage (10 × 19 × 11 in., 190 in^2 floor space). We chose 3-month-old female mice since by 5 months of age most of the trabecular bone is gone, while sufficient for quantitation at 3 months. They show 15%–50% lower values in trabecular bone parameters compared to 5-month-old male mice. The animals were weight-matched (male/control, 34.11 ± 4.20 g; L-BAIBA, 34.35 ± 4.23 g; female/control, 21.54 ± 1.08 g; L-BAIBA, 21.37 ± 1.88 g). L-BAIBA (100 mg/kg/day, AdipoGen Life Sciences) was provided in drinking water *ad libitum*, and the amounts consumed were similar in both control (male, 7.76 ± 0.55 mL; female, 6.88 ± 0.08 mL) and treated mice (male, 8.13 ± 0.73 mL; female, 6.97 ± 0.06 mL). L-BAIBA intake was 106.75 ± 12.04 and 129.91 ± 6.24 mg/kg/day for male and female, respectively. Hindlimb unloading was carried out for 2 weeks as described previously (Ferreira et al., 2011), with some modifications (Maurel et al., 2016). Mice were suspended by a tail ring surgically inserted through inter-vertebral disc space. The tail ring was attached to the tail with a supportive steel wire by strips of adhesive tape for reinforcement. This system allows a 360-degree range of motion while maintaining approximately a 30-degree angle between the body axis and cage bottom to prevent the contact of hindlimbs to the floor.

After 2 weeks of hindlimb unloading, EDL and soleus were dissected for *ex vivo* muscle contractility analysis. The right tibia was dissected for *ex vivo* μCT and the left tibia for bone histomorphometry. Both femurs were used for real-time PCR after flushing bone marrow.

Live Imaging of Osteocyte Mitochondria

Confocal imaging of cultured osteocytes was conducted using a Leica TCS SP8 confocal microscope equipped with a 40×, 1.2W (water immersion) objective. Primary bone osteocytes from DMP1-GFP mice or MLO-Y4 cells were incubated with 200 nM

MitoTracker Deep Red FM (Invitrogen, M22426) for 30 min at 37°C, for visualization of mitochondrial morphology and dynamics, or incubated with 50 nM TMRE (Invitrogen, T669) for 10 min at 37°C, for monitoring mitochondrial inner membrane potential as previously described (Wang et al., 2018; Yi et al., 2011; Zhou et al., 2010). MitoTracker Deep Red FM was excited at 633 nm and its emitted fluorescence was collected at 640–690 nm. TMRE was excited at 543 nm with the fluorescence collected at 560–620 nm. The live-cell imaging was conducted at room temperature. NIH ImageJ software was used for imaging processing and quantification of the fluorescence intensity of TMRE and MitoTracker Deep Red.

Statistical Analysis

Data were expressed as means ± SD. The statistical significance of the difference between mean values was determined by the following statistical methods, using Prism 7.0 (GraphPad) or IBM SSPS Statistics: muscle CM analysis, multifactorial ANOVA followed by simple effect test with least significant difference (LSD); μCT and bone histomorphometry analyses, one-tailed paired t test for analyzing *in vivo* and *ex vivo* μCT and bone histomorphometry data and paired t test or two-way ANOVA followed by sidak post hoc test for EF classification; muscle contraction analysis, data were statistically analyzed with one-tailed paired t test and two-way ANOVA followed by sidak post hoc test; quantification of cell death and ROS, one-way ANOVA followed by tukey post hoc test; real-time qPCR, one-tailed paired t test or multifactorial ANOVA followed by simple effect test with LSD. Differences were considered significant at $p < 0.05$.

Data and Accessibility

The original raw data this work have been deposited at Mendeley Data and are available at https://doi.org/10.17632/gydsk6dvm2.1

Supplementary Material

Refer to Web version on PubMed Central for supplementary material.

Acknowledgments

We thank Mark Dallas for his help with the μCT measurements and Carrie Zhao for her assistance with maintenance of the mice. We thank Keith W. Condon and Lilian I. Plotkin for their advice regarding bone histomorphometric analysis. This work was supported by NIH NIA P1PO1AG039355 (L.F.B.), the Histology Core of the Indiana Center for Musculoskeletal Health (ICMH) at IU School of Medicine, and the Bone and Body Composition Core of the Indiana Clinical Translational Sciences Institute (CTSI) from NIH NCATS CTSA UL1TR001108. J.Z. received support from NIH NIAMS R01 AR057404 and Bank of American Victor E. Speas Foundation.

References

Almeida M, O'Brien CA. Basic biology of skeletal aging: role of stress response pathways. J Gerontol A Biol Sci Med Sci. 2013; 68:1197–1208. [PubMed: 23825036]

Bakewell L, Burdge GC, Calder PC. Polyunsaturated fatty acid concentrations in young men and women consuming their habitual diets. Br J Nutr. 2006; 96:93–99. [PubMed: 16869996]

Basso N, Heersche JN. Effects of hind limb unloading and reloading on nitric oxide synthase expression and apoptosis of osteocytes and chondrocytes. Bone. 2006; 39:807–814. [PubMed: 16765658]

Begriche K, Massart J, Abbey-Toby A, Igoudjil A, Lettéron P, Fromenty B. Beta-aminoisobutyric acid prevents diet-induced obesity in mice with partial leptin deficiency. Obesity (Silver Spring). 2008; 16:2053–2067. [PubMed: 19186330]

Bellido T, Plotkin LI. Novel actions of bisphosphonates in bone: preservation of osteoblast and osteocyte viability. Bone. 2011; 49:50–55. [PubMed: 20727997]

Benefield LE, Holtzclaw BJ. Aging in place: merging desire with reality. Nurs Clin North Am. 2014; 49:123–131. [PubMed: 24846462]

Blair SN, Kohl HW 3rd, Barlow CE, Paffenbarger RS Jr, Gibbons LW, Macera CA. Changes in physical fitness and all-cause mortality. A prospective study of healthy and unhealthy men. JAMA. 1995; 273:1093–1098. [PubMed: 7707596]

Bonewald LF. The amazing osteocyte. J Bone Miner Res. 2011; 26:229–238. [PubMed: 21254230]

Bonewald LF, Kiel DP, Clemens TL, Esser K, Orwoll ES, O'Keefe RJ, Fielding RA. Forum on bone and skeletal muscle interactions: summary of the proceedings of an ASBMR workshop. J Bone Miner Res. 2013; 28:1857–1865. [PubMed: 23671010]

Brotto M, Bonewald L. Bone and muscle: Interactions beyond mechanical. Bone. 2015; 80:109–114. [PubMed: 26453500]

Cabahug-Zuckerman P, Frikha-Benayed D, Majeska RJ, Tuthill A, Yakar S, Judex S, Schaffler MB. Osteocyte Apoptosis Caused by Hindlimb Unloading is Required to Trigger Osteocyte RANKL Production and Subsequent Resorption of Cortical and Trabecular Bone in Mice Femurs. J Bone Miner Res. 2016; 31:1356–1365. [PubMed: 26852281]

Cavanaugh DJ, Lee H, Lo L, Shields SD, Zylka MJ, Basbaum AI, Anderson DJ. Distinct subsets of unmyelinated primary sensory fibers mediate behavioral responses to noxious thermal and mechanical stimuli. Proc Natl Acad Sci USA. 2009; 106:9075–9080. [PubMed: 19451647]

Colaianni G, Cuscito C, Mongelli T, Pignataro P, Buccoliero C, Liu P, Lu P, Sartini L, Di Comite M, Mori G, et al. The myokine irisin increases cortical bone mass. Proc Natl Acad Sci USA. 2015; 112:12157–12162. [PubMed: 26374841]

Dallas SL, Prideaux M, Bonewald LF. The osteocyte: an endocrine cell… and more. Endocr Rev. 2013; 34:658–690. [PubMed: 23612223]

Dankbar B, Fennen M, Brunert D, Hayer S, Frank S, Wehmeyer C, Beckmann D, Paruzel P, Bertrand J, Redlich K, et al. Myostatin is a direct regulator of osteoclast differentiation and its inhibition reduces inflammatory joint destruction in mice. Nat Med. 2015; 21:1085–1090. [PubMed: 26236992]

Edwards RH, Hill DK, Jones DA, Merton PA. Fatigue of long duration in human skeletal muscle after exercise. J Physiol. 1977a; 272:769–778. [PubMed: 592214]

Edwards RH, Young A, Hosking GP, Jones DA. Human skeletal muscle function: description of tests and normal values. Clin Sci Mol Med. 1977b; 52:283–290. [PubMed: 844260]

Ehrenborg E, Krook A. Regulation of skeletal muscle physiology and metabolism by peroxisome proliferator-activated receptor delta. Pharmacol Rev. 2009; 61:373–393. [PubMed: 19805479]

Feng JQ, Huang H, Lu Y, Ye L, Xie Y, Tsutsui TW, Kunieda T, Castranio T, Scott G, Bonewald LB, Mishina Y. The Dentin matrix protein 1 (Dmp1) is specifically expressed in mineralized, but not soft, tissues during development. J Dent Res. 2003; 82:776–780. [PubMed: 14514755]

Ferreira JA, Crissey JM, Brown M. An alternant method to the traditional NASA hindlimb unloading model in mice. J Vis Exp. 2011; 49:2467.

Finkel T. The metabolic regulation of aging. Nat Med. 2015; 21:1416–1423. [PubMed: 26646498]

Frikha-Benayed D, Basta-Pljakic J, Majeska RJ, Schaffler MB. Regional differences in oxidative metabolism and mitochondrial activity among cortical bone osteocytes. Bone. 2016; 90:15–22. [PubMed: 27260646]

Giltay EJ, Gooren LJ, Toorians AW, Katan MB, Zock PL. Docosahexaenoic acid concentrations are higher in women than in men because of estrogenic effects. Am J Clin Nutr. 2004; 80:1167–1174. [PubMed: 15531662]

Hamrick MW, McNeil PL, Patterson SL. Role of muscle-derived growth factors in bone formation. J Musculoskelet Neuronal Interact. 2010; 10:64–70. [PubMed: 20190381]

Holzerová E, Prokisch H. Mitochondria: Much ado about nothing? How dangerous is reactive oxygen species production? Int J Biochem Cell Biol. 2015; 63:16–20. [PubMed: 25666559]

Huang J, Romero-Suarez S, Lara N, Mo C, Kaja S, Brotto L, Dallas SL, Johnson ML, Jähn K, Bonewald LF, Brotto M. Crosstalk between MLO-Y4 osteocytes and C2C12 muscle cells is mediated by the Wnt/β-catenin pathway. JBMR Plus. 2017; 1:86–100. [PubMed: 29104955]

Jähn K, Lara-Castillo N, Brotto L, Mo CL, Johnson ML, Brotto M, Bonewald LF. Skeletal muscle secreted factors prevent glucocorticoid-induced osteocyte apoptosis through activation of β-catenin. Eur Cell Mater. 2012; 24:197–209. discussion 209–210. [PubMed: 22972510]

Jilka RL, O'Brien CA. The Role of Osteocytes in Age-Related Bone Loss. Curr Osteoporos Rep. 2016; 14:16–25. [PubMed: 26909563]

Jilka RL, Noble B, Weinstein RS. Osteocyte apoptosis. Bone. 2013; 54:264–271. [PubMed: 23238124]

Joeng KS, Lee YC, Lim J, Chen Y, Jiang MM, Munivez E, Ambrose C, Lee BH. Osteocyte-specific WNT1 regulates osteoblast function during bone homeostasis. J Clin Invest. 2017; 127:2678–2688. [PubMed: 28628032]

Jung TW, Hwang HJ, Hong HC, Yoo HJ, Baik SH, Choi KM. BAIBA attenuates insulin resistance and inflammation induced by palmitate or a high fat diet via an AMPK-PPARδ-dependent pathway in mice. Diabetologia. 2015; 58:2096–2105. [PubMed: 26105792]

Karsenty G, Olson EN. Bone and Muscle Endocrine Functions: Unexpected Paradigms of Inter-organ Communication. Cell. 2016; 164:1248–1256. [PubMed: 26967290]

Kato Y, Windle JJ, Koop BA, Mundy GR, Bonewald LF. Establishment of an osteocyte-like cell line, MLO-Y4. J Bone Miner Res. 1997; 12:2014–2023. [PubMed: 9421234]

Kennedy OD, Herman BC, Laudier DM, Majeska RJ, Sun HB, Schaffler MB. Activation of resorption in fatigue-loaded bone involves both apoptosis and active pro-osteoclastogenic signaling by distinct osteocyte populations. Bone. 2012; 50:1115–1122. [PubMed: 22342796]

Kitase Y, Barragan L, Qing H, Kondoh S, Jiang JX, Johnson ML, Bonewald LF. Mechanical induction of PGE2 in osteocytes blocks glucocorticoid-induced apoptosis through both the β-catenin and PKA pathways. J Bone Miner Res. 2010; 25:2657–2668. [PubMed: 20578217]

Langlais C, Hughes MA, Cain K, MacFarlane M. In Vitro Assembly and Analysis of the Apoptosome Complex. Cold Spring Harb Protoc. 2015; 2015 pdb.prot087080.

Manolagas SC, Parfitt AM. For whom the bell tolls: distress signals from long-lived osteocytes and the pathogenesis of metabolic bone diseases. Bone. 2013; 54:272–278. [PubMed: 23010104]

Maurel DB, Duan P, Farr J, Cheng AL, Johnson ML, Bonewald LF. Beta-Catenin Haplo Insufficient Male Mice Do Not Lose Bone in Response to Hindlimb Unloading. PLoS ONE. 2016; 11:e0158381. [PubMed: 27410430]

McNeil, B., Dong, X. Mrgprs as Itch Receptors. In: Carstens, E., Akiyama, T., editors. Itch: Mechanisms and Treatment. CRC Press/Taylor & Francis; 2014. Chapter 12https://www.ncbi.nlm.nih.gov/books/NBK200929/

Mo C, Romero-Suarez S, Bonewald L, Johnson M, Brotto M. Prostaglandin E2: from clinical applications to its potential role in bone-muscle crosstalk and myogenic differentiation. Recent Pat Biotechnol. 2012; 6:223–229. [PubMed: 23092433]

Nakashima T, Hayashi M, Fukunaga T, Kurata K, Oh-Hora M, Feng JQ, Bonewald LF, Kodama T, Wutz A, Wagner EF, et al. Evidence for osteocyte regulation of bone homeostasis through RANKL expression. Nat Med. 2011; 17:1231–1234. [PubMed: 21909105]

Nielsen AR, Mounier R, Plomgaard P, Mortensen OH, Penkowa M, Speerschneider T, Pilegaard H, Pedersen BK. Expression of interleukin-15 in human skeletal muscle effect of exercise and muscle fibre type composition. J Physiol. 2007; 584:305–312. [PubMed: 17690139]

Pedersen BK. Muscles and their myokines. J Exp Biol. 2011; 214:337–346. [PubMed: 21177953]

Qin Y, Peng Y, Zhao W, Pan J, Ksiezak-Reding H, Cardozo C, Wu Y, Divieti Pajevic P, Bonewald LF, Bauman WA, Qin W. Myostatin inhibits osteoblastic differentiation by suppressing osteocyte-derived exosomal microRNA-218: A novel mechanism in muscle-bone communication. J Biol Chem. 2017; 292:11021–11033. [PubMed: 28465350]

Rinholm JE, Vervaeke K, Tadross MR, Tkachuk AN, Kopek BG, Brown TA, Bergersen LH, Clayton DA. Movement and structure of mitochondria in oligodendrocytes and their myelin sheaths. Glia. 2016; 64:810–825. [PubMed: 26775288]

Roberts LD, Boström P, O'Sullivan JF, Schinzel RT, Lewis GD, Dejam A, Lee YK, Palma MJ, Calhoun S, Georgiadi A, et al. β-Aminoisobutyric acid induces browning of white fat and hepatic β-oxidation and is inversely correlated with cardiometabolic risk factors. Cell Metab. 2014; 19:96–108. [PubMed: 24411942]

Shi CX, Zhao MX, Shu XD, Xiong XQ, Wang JJ, Gao XY, Chen Q, Li YH, Kang YM, Zhu GQ. β-aminoisobutyric acid attenuates hepatic endoplasmic reticulum stress and glucose/lipid metabolic disturbance in mice with type 2 diabetes. Sci Rep. 2016; 6:21924. [PubMed: 26907958]

Shinohara T, Harada M, Ogi K, Maruyama M, Fujii R, Tanaka H, Fukusumi S, Komatsu H, Hosoya M, Noguchi Y, et al. Identification of a G protein-coupled receptor specifically responsive to beta-alanine. J Biol Chem. 2004; 279:23559–23564. [PubMed: 15037633]

Smith H, Dymond B. The Determination of Beta-Amino-Isobutyric Acid in Urine. Clin Chim Acta. 1963; 8:614–620. [PubMed: 14063978]

Stern AR, Stern MM, Van Dyke ME, Jähn K, Prideaux M, Bonewald LF. Isolation and culture of primary osteocytes from the long bones of skeletally mature and aged mice. Biotechniques. 2012; 52:361–373. [PubMed: 22668415]

Uno M, Nishimura S, Fukuchi K, Kaneta Y, Oda Y, Komori H, Takeda S, Haga T, Agatsuma T, Nara F. Identification of physiologically active substances as novel ligands for MRGPRD. J Biomed Biotechnol. 2012; 2012:816159. [PubMed: 23091359]

Urakawa I, Yamazaki Y, Shimada T, Iijima K, Hasegawa H, Okawa K, Fujita T, Fukumoto S, Yamashita T. Klotho converts canonical FGF receptor into a specific receptor for FGF23. Nature. 2006; 444:770–774. [PubMed: 17086194]

Valko M, Leibfritz D, Moncol J, Cronin MT, Mazur M, Telser J. Free radicals and antioxidants in normal physiological functions and human disease. Int J Biochem Cell Biol. 2007; 39:44–84. [PubMed: 16978905]

van Bezooijen RL, Roelen BA, Visser A, van der Wee-Pals L, de Wilt E, Karperien M, Hamersma H, Papapoulos SE, ten Dijke P, Löwik CW. Sclerostin is an osteocyte-expressed negative regulator of bone formation, but not a classical BMP antagonist. J Exp Med. 2004; 199:805–814. [PubMed: 15024046]

Vemula H, Kitase Y, Ayon NJ, Bonewald L, Gutheil WG. Gaussian and linear deconvolution of LC-MS/MS chromatograms of the eight aminobutyric acid isomers. Anal Biochem. 2017; 516:75–85. [PubMed: 27771391]

Verborgt O, Gibson GJ, Schaffler MB. Loss of osteocyte integrity in association with microdamage and bone remodeling after fatigue in vivo. J Bone Miner Res. 2000; 15:60–67. [PubMed: 10646115]

Verborgt O, Tatton NA, Majeska RJ, Schaffler MB. Spatial distribution of Bax and Bcl-2 in osteocytes after bone fatigue: complementary roles in bone remodeling regulation? J Bone Miner Res. 2002; 17:907–914. [PubMed: 12009022]

Wang H, Qian J, Zhao X, Xing C, Sun B. β-Aminoisobutyric acid ameliorates the renal fibrosis in mouse obstructed kidneys via inhibition of renal fibroblast activation and fibrosis. J Pharmacol Sci. 2017; 133:203–213. [PubMed: 28433566]

Wang H, Yi J, Li X, Xiao Y, Dhakal K, Zhou J. ALS-associated mutation SOD1G93A leads to abnormal mitochondrial dynamics in osteocytes. Bone. 2018; 106:126–138. [PubMed: 29030231]

Xiong J, Piemontese M, Onal M, Campbell J, Goellner JJ, Dusevich V, Bonewald L, Manolagas SC, O'Brien CA. Osteocytes, not Osteoblasts or Lining Cells, are the Main Source of the RANKL Required for Osteoclast Formation in Remodeling Bone. PLoS ONE. 2015; 10:e0138189. [PubMed: 26393791]

Yi J, Ma C, Li Y, Weisleder N, Ríos E, Ma J, Zhou J. Mitochondrial calcium uptake regulates rapid calcium transients in skeletal muscle during excitation-contraction (E-C) coupling. J Biol Chem. 2011; 286:32436–32443. [PubMed: 21795684]

Zhou J, Yi J, Fu R, Liu E, Siddique T, Ríos E, Deng HX. Hyperactive intracellular calcium signaling associated with localized mitochondrial defects in skeletal muscle of an animal model of amyotrophic lateral sclerosis. J Biol Chem. 2010; 285:705–712. [PubMed: 19889637]

Zylka MJ, Rice FL, Anderson DJ. Topographically distinct epidermal nociceptive circuits revealed by axonal tracers targeted to Mrgprd. Neuron. 2005; 45:17–25. [PubMed: 15629699]

Highlights

- The muscle metabolite L-BAIBA protects osteocytes from ROS-induced cell death
- L-BAIBA prevents mitochondrial breakdown in osteocytes
- The effects of L-BAIBA are mediated via MRGPRD that decreases with aging
- *In vivo*, L-BAIBA reduces bone and muscle loss resulting from immobilization

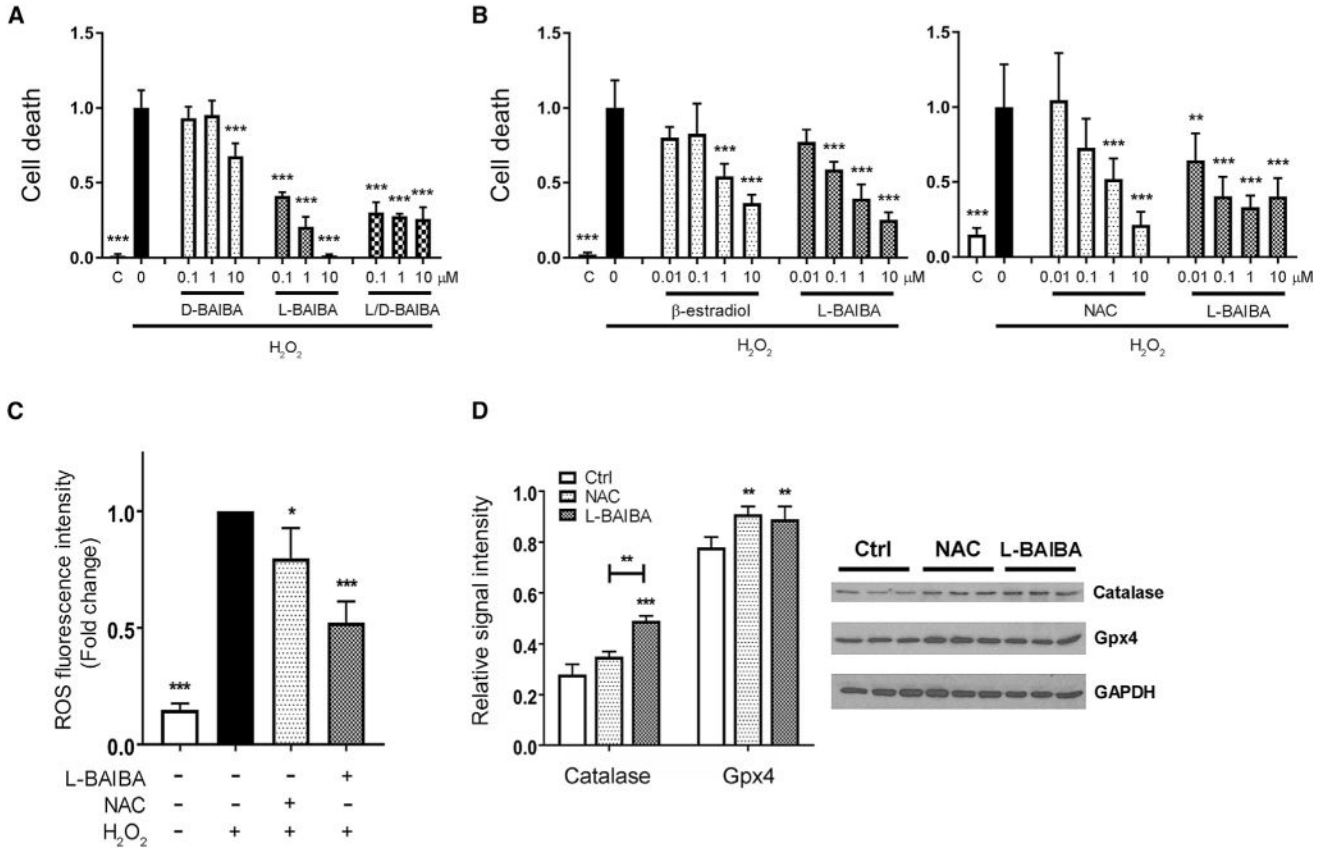

Figure 1. L-BAIBA Protects Osteocytes from Cell Death Induced by Oxidative Stress

(A) Cell death assay using the osteocyte cell line MLO-Y4. L-BAIBA as well as L/D-BAIBA, but not D-BAIBA, showed highly significant protective effects on MLO-Y4 cell death induced by oxidative stress. ***$p < 0.001$ versus H_2O_2.

(B) Comparison of potency between L-BAIBA and well-known antioxidants β-estradiol and N-acetylcysteine (NAC) on MLO-Y4 cell death induced by oxidative stress. **$p < 0.01$ and ***$p < 0.001$ versus H_2O_2.

(C) Prevention by L-BAIBA of reactive oxygen species (ROS) generation induced by oxidative stress. *$p < 0.05$ and ***$p < 0.001$ versus H_2O_2.

(D) Induction of antioxidant enzymes, catalase, and Gpx4 by L-BAIBA. **$p < 0.01$ and ***$p < 0.001$ versus control.

The data are expressed as the mean ± SD. See also Figures S1–S3.

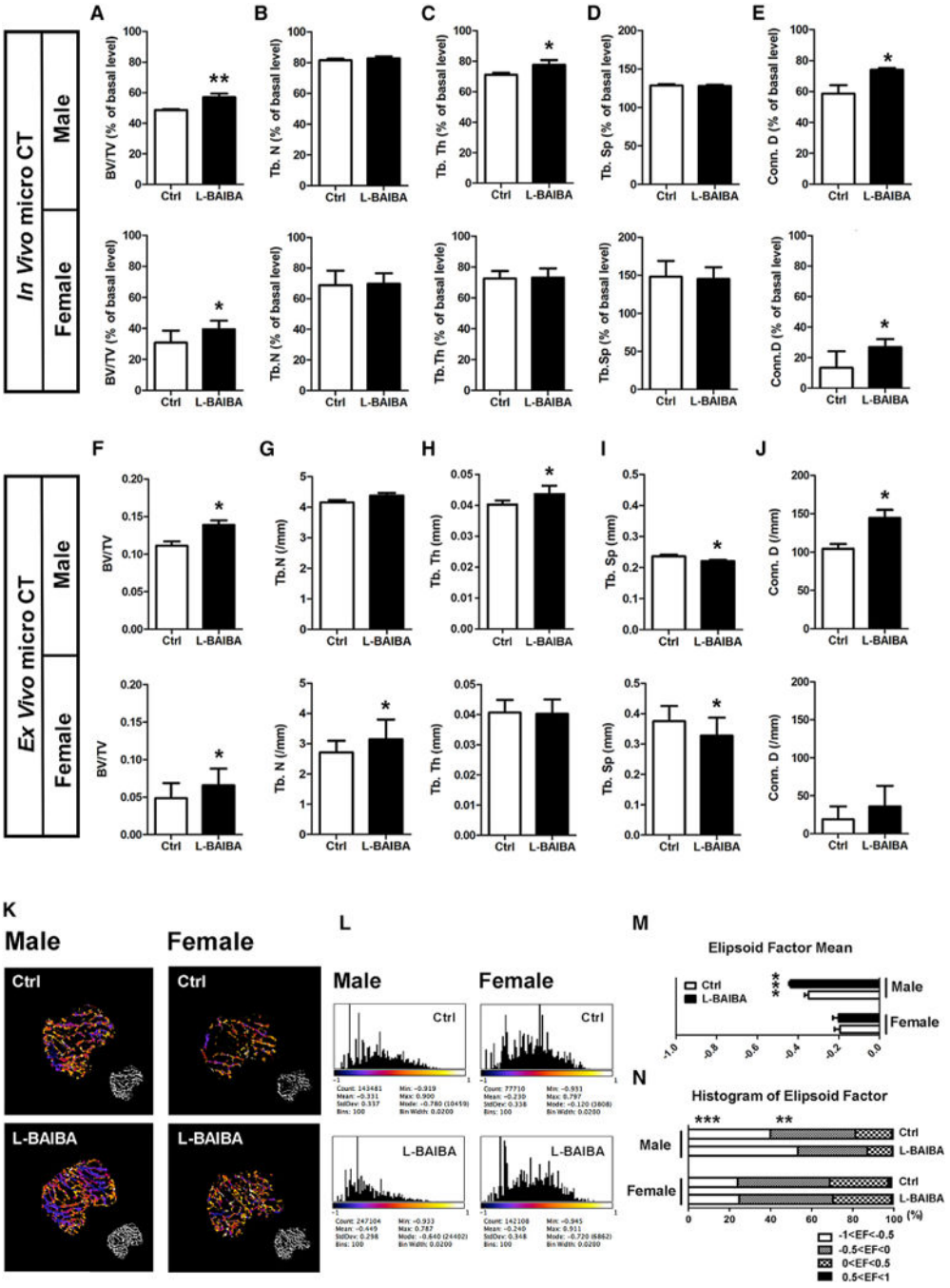

Figure 2. L-BAIBA Maintains Trabecular Bone Mass and Connectivity after 2 Weeks of Hindlimb Unloading

(A–J) μCT analysis of cancellous bones in right proximal tibiae, *in vivo* (A–E) and *ex vivo* (F–J). Bone volume fraction (BV/TV) (A and F), trabecular number (Tb.N) (B and G), trabecular thickness (Tb.Th) (C and H), trabecular separation (Tb.Sp) (D and I), and connectivity density (Conn.D) (E and J) were examined. Upper panel is for the 5-month-old male (n = 6) and lower panel is for the 3-month-old female (n = 6). All the parameters *in vivo* μCT are expressed as a percentage of baseline. *$p < 0.05$ and **$p < 0.01$ versus control.

(K–N) Ellipsoid factor (EF) classification for rod/plate geometry. Representative 3D color map images of control and L-BAIBA (K) indicate EF > 0 in orange-yellow (rod type) and EF < 0 in purple-blue (plate type). Corresponding EF histograms of control and L-BAIBA (L) indicate a shift to the left for plate-dominated structures and to the right for rod-dominated structures. Mean of EF (M) and summary of EF histograms (N) are shown. 5-month-old male, n = 6; 3-month-old female, n = 6. **p < 0.01 and ***p < 0.001 versus control.

The data are expressed as the mean ± SD.

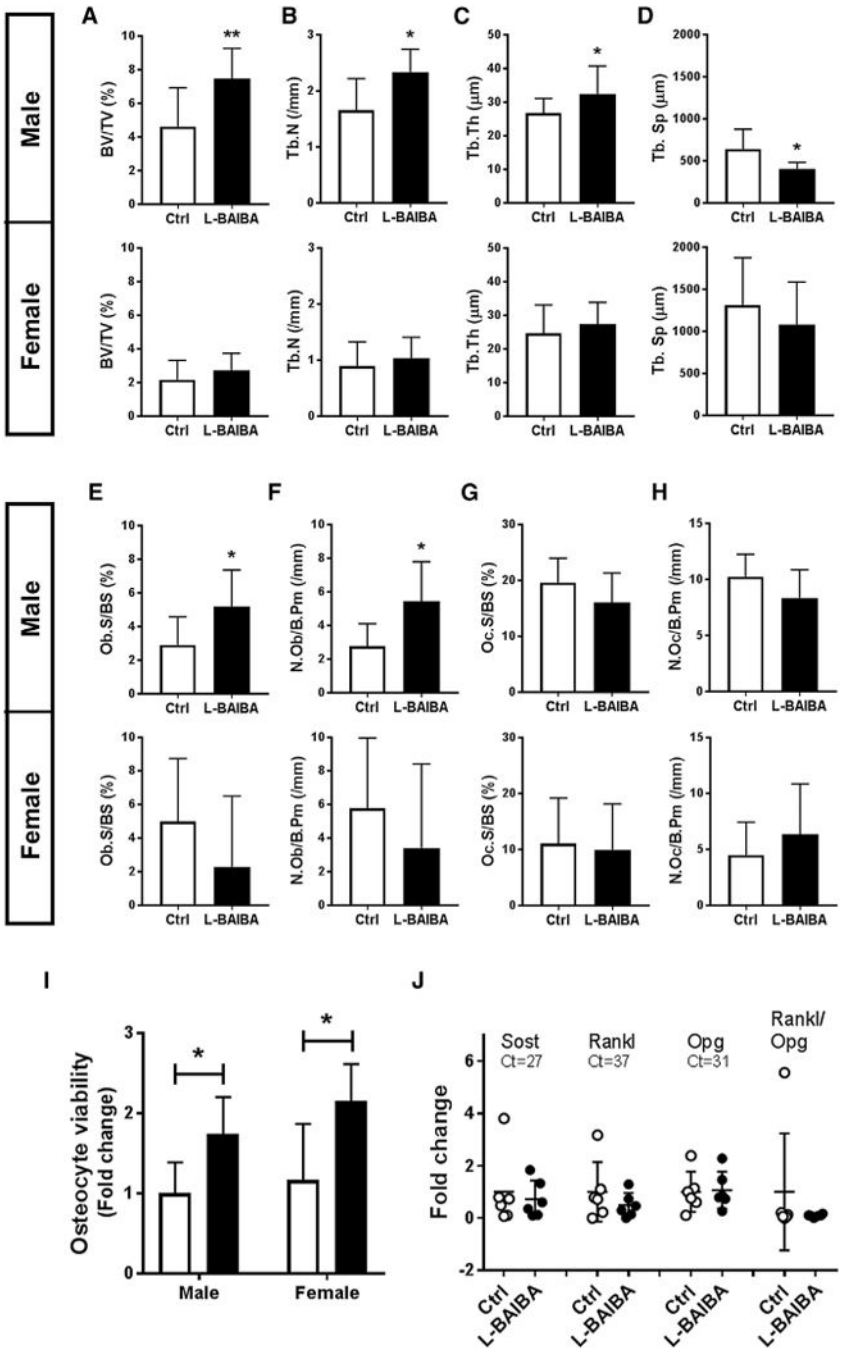

Figure 3. L-BAIBA Maintains Trabecular Bone Mass and Osteocyte Viability after 2 Weeks of Hindlimb Unloading

(A–H) Bone static histomorphometry of cancellous bones in left proximal tibiae, *in vivo*. Bone volume fraction (BV/TV) (A), trabecular number (Tb.N) (B), trabecular thickness (Tb.Th) (C), trabecular separation (Tb.Sp) (D), osteoblast surface (Ob.S/BS) (E), osteoblast number (N.Ob/B.Pm) (F), osteoclast surface (Oc.S/BS) (G), and osteoclast number (N.Oc/B.Pm) (H) were examined. Upper panel is for the 5-month-old male (n = 6) and lower panel is for the 3-month-old female (n = 6). *$p < 0.05$ and **$p < 0.01$ versus control.

(I) Osteocyte viability evaluated by TUNEL apoptosis assay with 5-month-old male (n = 6) and 3-month-old female (n = 6). *$p < 0.05$ versus control.
(J) Real-time qPCR analysis of Sost, Rankl, and Opg mRNA expression in femurs obtained from hindlimb unloaded male mice (n = 6). Data are expressed as fold change over the expression level of each gene in control mice (average Ct value is 27 for Sost, 37 for Rankl, and 31 for Opg). No significant difference was detected compared to control.
The data are expressed as the mean ± SD.

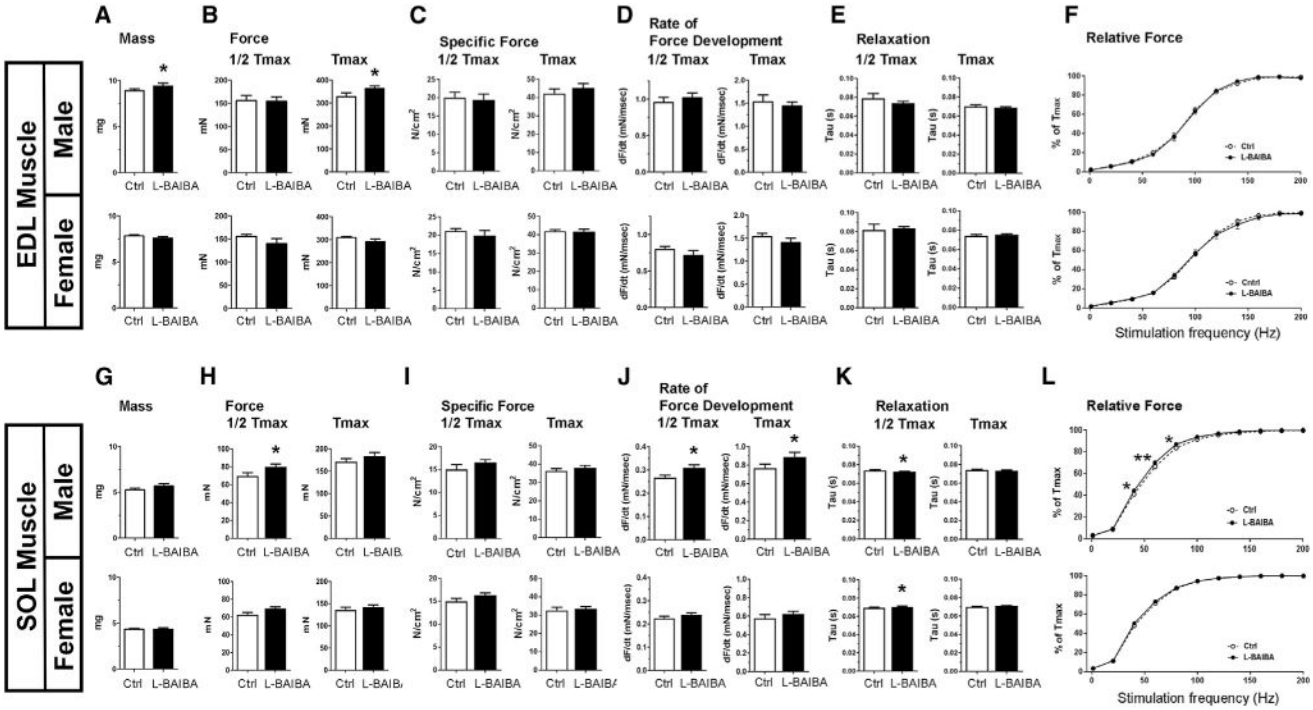

Figure 4. L-BAIBA Maintains EDL and Soleus Muscle Function after 2 Weeks of Hindlimb Unloading

(A–L) EDL and soleus muscle functional analysis, EDL (A–F) and soleus (G–L). Half-maximal (1/2 Tmax) and maximal tetanic contractions (Tmax) are shown in left and right panels, respectively. Upper panel is for the 5-month-old male (n = 6) and lower panel is for the 3-month-old female (n = 6). Muscle mass (A and G), muscle force (B and H), muscle-specific force (C and I), muscle rate of contractile force development (D and J), muscle relaxation (E and K), and muscle relative force (F and L) are examined. Relative force is a force versus frequency relationship among the stimulatory frequencies of 1–200 Hz, wherein force at each frequency is expressed as a percentage of Tmax. *$p < 0.05$ and **$p < 0.01$ versus control.

The data are expressed as the mean ± SD.

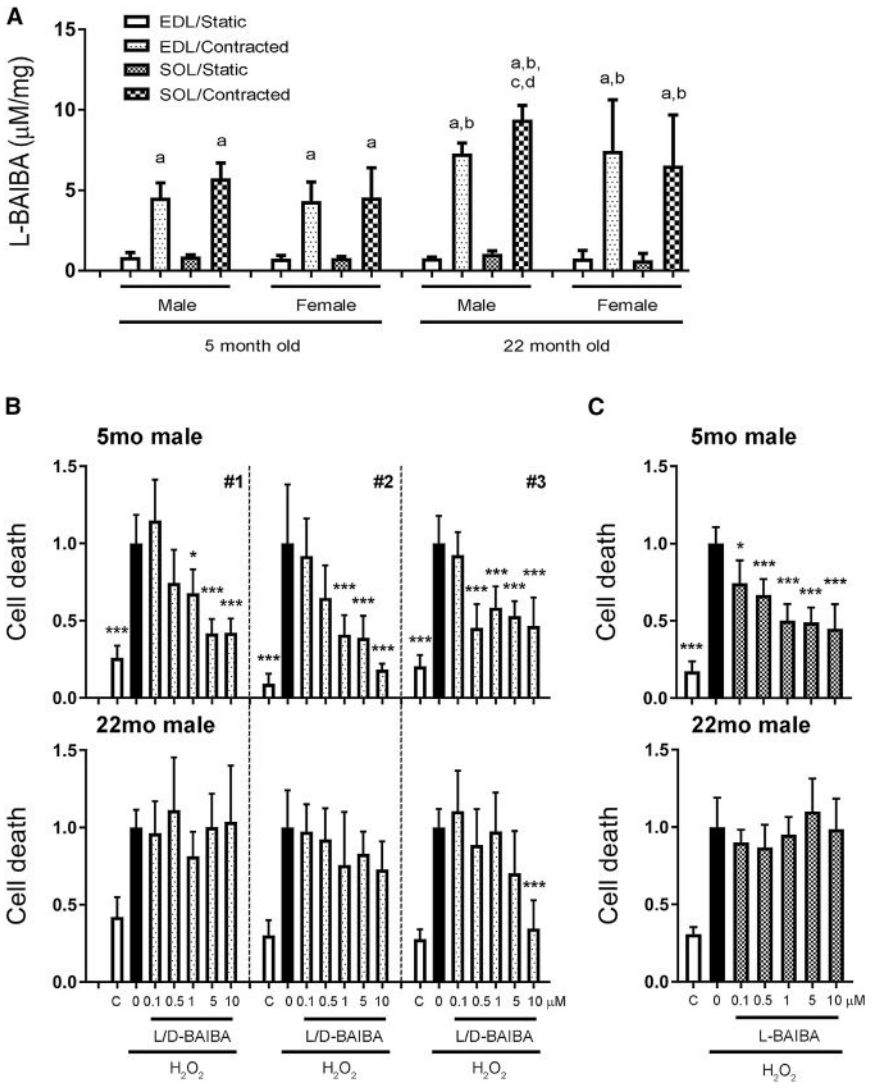

Figure 5. L-BAIBA Is Secreted by Both Young and Old Contracted Muscle but Only Protects Young, but Not Old, Primary Osteocytes from Cell Death Induced by Oxidative Stress

(A) L-BAIBA production by *ex vivo* contracted muscle at 90 Hz. The amount of L-BAIBA was normalized by muscle mass. a, versus corresponding non-contracted muscle CM; b, versus corresponding contracted muscle CM obtained from 5-month-old mice; c, versus corresponding contracted muscle CM obtained from female mice; d, versus contracted EDL muscle CM obtained from 22-month-old male mice; $p < 0.05$.

(B and C) Cell death assay of primary bone cells from long bones. L/D-BAIBA (B) and L-BAIBA (C) protect primary bone cells obtained from 5-month-old male mice (upper panel) under oxidative stress, but not the ones from 22-month-old male mice (lower panel). *$p < 0.05$ and ***$p < 0.001$ versus H_2O_2.

The data are expressed as the mean ± SD. See also Figure S4.

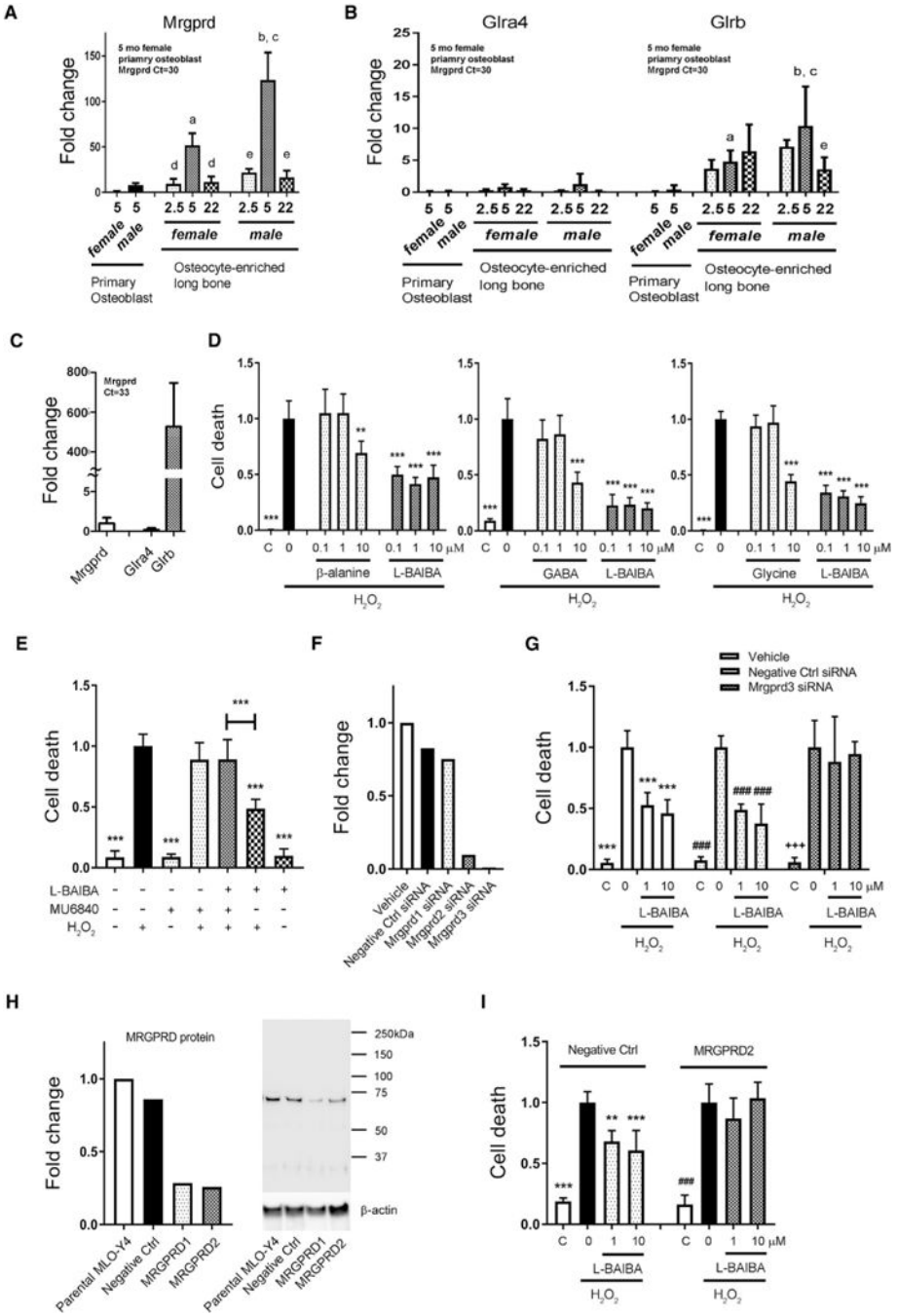

Figure 6. The Protective Effects of L-BAIBA on Osteocyte Viability Are Mediated through the MRGPRD

(A and B) Real-time qPCR analysis of *Mrgprd* (A) and Glra4/b (B) mRNA expression in primary osteoblast fractions and osteocyte-enriched bones obtained from male and female at 2.5, 5, and 22 months old. Data are expressed as fold change over the *Mrgprd* expression level in primary osteoblast fractions obtained from 5-month-old female mice (average Ct value is 30). *Glra1–3* are undetectable. a, versus 5-month-old female primary osteoblast fraction (pObF); b, versus 5-month-old male pObF; c, versus 5-month-old female osteocyte-

enriched bones (pOcyB); d, versus 5-month-old female pOcyB; e, versus 5-month-old male pOcyB; $p < 0.05$.

(C) Real-time qPCR analysis of *Mrgprd* and *Glra4/b* mRNA expression in MLO-Y4 cells. Data are expressed as fold change over the *Mrgprd* expression level (average Ct value is 33). *Glra1–3* are undetectable.

(D) Comparison of L-BAIBA with other MRGPRD ligands, β-alanine, GABA, and glycine in cell death assay. **$p < 0.01$ and ***$p < 0.001$ versus H_2O_2.

(E) An antagonist against MRGPRD, MU6840 prevents the protective effect of L-BAIBA on osteocyte viability. ***$p < 0.001$ versus H_2O_2.

(F) Real-time qPCR analysis to determine the efficiency of *Mrgprd* knockdown using RNAi system. Data are expressed as fold change over the expression level in parental MLO-Y4.

(G) *Mrgprd* knockdown by siRNA prevents the protective effect of L-BAIBA on osteocyte viability. ***$p < 0.001$ versus vehicle/H_2O_2, ###$p < 0.001$ versus negative control/H_2O_2, and +++$p < 0.001$ versus *Mrgprd* siRNA/H_2O_2.

(H) Western blot analysis to determine the efficiency of *Mrgprd* knockout using CRISPR/Cas9 system. Data are normalized by β-actin and expressed as fold change over the expression level in parental MLO-Y4.

(I) *Mrgprd* knockout by CRISPR/Cas9 prevents the protective effect of L-BAIBA on osteocyte viability. **$p < 0.01$ and ***$p < 0.001$ versus negative control/H_2O_2 and ###$p < 0.001$ versus MRGPRD2/H_2O_2.

The data are expressed as the mean ± SD.

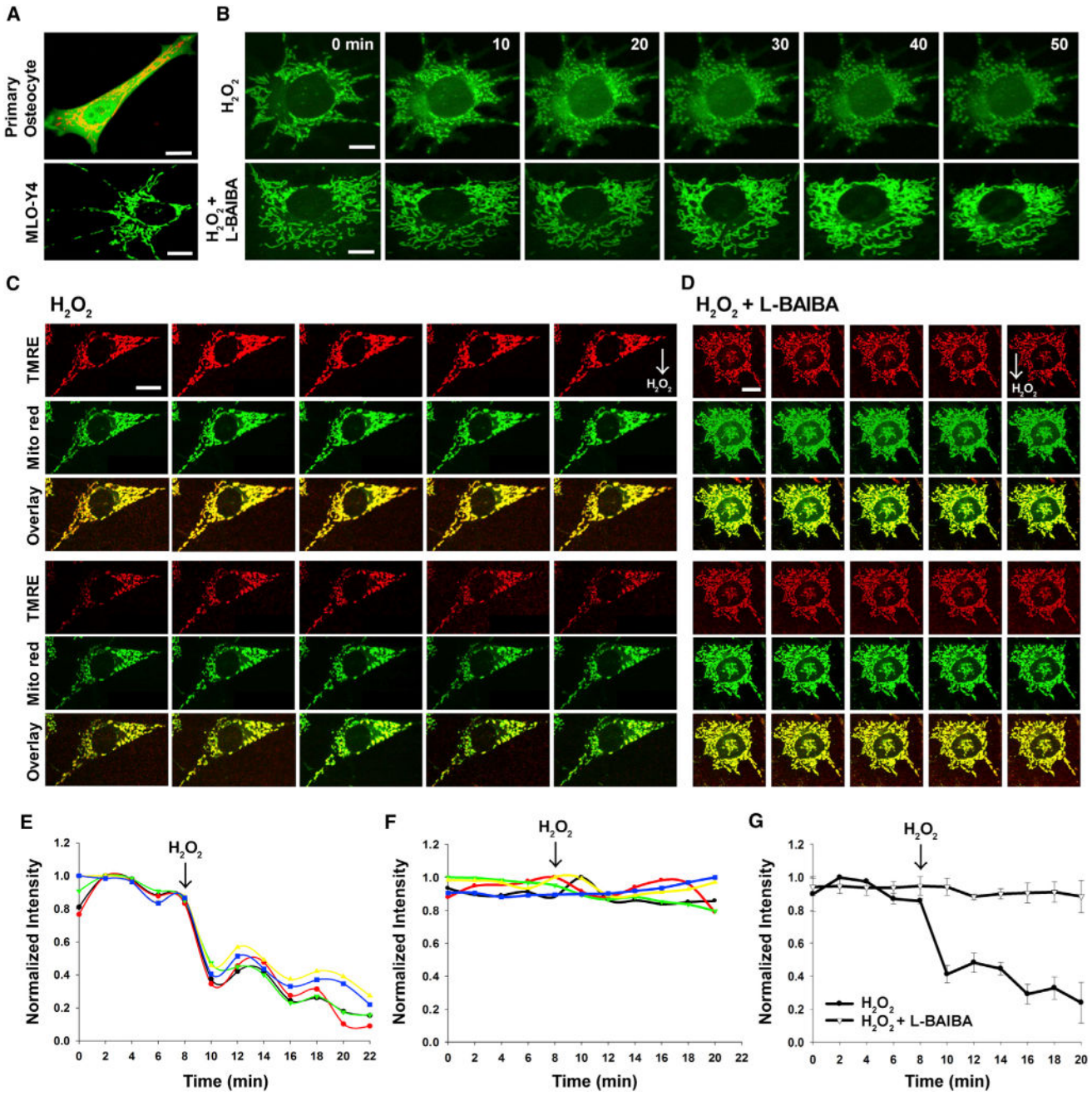

Figure 7. Confocal Microscopy Images of Mitochondrial Response to Acute Treatment of Hydrogen Peroxide in Live Cells, Prevention of Mitochondrial Breakdown by L-BAIBA

(A) Mitochondria in a primary osteocyte (top) and a MLO-Y4 cell (bottom).

(B) Time-lapse confocal imaging of mitochondria in MLO-Y4 cell after treatment with hydrogen peroxide (100 μM) alone (top row) and with 100 μM hydrogen peroxide plus L-BAIBA (bottom row).

(C and D) Evaluation of mitochondrial membrane potential using TMRE (red) and structure using Mito Red (green) with the treatment of hydrogen peroxide alone (C) and of hydrogen peroxide plus L-BAIBA (D). Arrow indicates the time that hydrogen peroxide was added.

(E–G) Quantification of the change of fluorescent intensity (TMRE) over the time per cell before and after treating with hydrogen peroxide (E), hydrogen peroxide plus L-BAIBA (F), and average fluorescence intensity of TMRE (n = 5) (G). Arrow indicates the time that hydrogen peroxide was added. Scale bar, 10 μm. See also Figure S5.